Diagnostic and Interventional Imaging 104 (2023) 142–152

Original article/*Research, New developments & Artificial Intelligence*

Predicting histopathology markers of endometrial carcinoma with a quantitative image analysis approach based on spherical harmonics in multiparametric MRI

Thierry L. Lefebvre[a,b], Ozan Ciga[c,d], Sahir Rai Bhatnagar[e,f,g], Yoshiko Ueno[e,h], Sameh Saif[e], Eric Winter-Reinhold[g], Anthony Dohan[i,j], Philippe Soyer[i,j], Reza Forghani[e,g], Kaleem Siddiqi[c], Jan Seuntjens[a], Caroline Reinhold[e,g,k,1], Peter Savadjiev[c,e,g,1,*]

[a] *Medical Physics Unit, McGill University, Montreal, QC H4A 3J1, Canada*
[b] *Cancer Research UK Cambridge Institute, University of Cambridge, Cambridge CB2 0RE, United Kingdom*
[c] *School of Computer Science and Centre for Intelligent Machines, McGill University, Montreal, QC H3A 2A7, Canada*
[d] *Department of Medical Biophysics, University of Toronto, Toronto ON M5G 1L7, Canada*
[e] *Department of Diagnostic Radiology, McGill University, Montreal, QC H4A 3J1, Canada*
[f] *Department of Epidemiology, Biostatistics and Occupational Health, McGill University, Montreal, QC H3A 1G1, Canada*
[g] *Augmented Intelligence & Precision Health Laboratory (AIPHL), Research Institute of McGill University Health Centre (RI-MUHC), Montreal, QC H4A 3J1, Canada*
[h] *Department of Radiology, Kobe University Graduate School of Medicine, Kobe City, Hyogo, 650-0017, Japan*
[i] *Department of Radiology, Hopital Cochin, AP-HP, 75014, Paris, France*
[j] *Université Paris Cité, Faculté de Médecine, 75006, Paris, France*
[k] *Montreal Imaging Experts Inc., Montreal, QC H9R 5K3, Canada*

ARTICLE INFO

Key Words:
Artificial intelligence
Endometrial cancer
Machine learning
Magnetic resonance imaging
Spherical harmonics (SPHARM)
Three-dimensional imaging

ABSTRACT

Purpose: Identifying optimal machine learning pipelines for computer-aided diagnosis is key for the development of robust, reproducible, and clinically relevant imaging biomarkers for endometrial carcinoma. The purpose of this study was to introduce the mathematical development of image descriptors computed from spherical harmonics (SPHARM) decompositions as well as the associated machine learning pipeline, and to evaluate their performance in predicting deep myometrial invasion (MI) and histopathological high-grade in preoperative multiparametric magnetic resonance imaging (MRI).

Patients and methods: This retrospective study included 128 women with histopathology-confirmed endometrial carcinomas who underwent 1.5-T MRI before hysterectomy between January 2011 and July 2015. SPHARM descriptors of each tumor were computed on multiparametric MRI images (T2-weighted, diffusion-weighted, dynamic contrast-enhanced-MRI and apparent diffusion coefficient maps). Tensor-based logistic regression was used to classify two-dimensional SPHARM rotationally-invariant descriptors. Head-to-head comparisons with radiomics analyses were performed with DeLong tests with Bonferroni-Holm correction to compare diagnostic performances.

Results: With all MRI contrasts, SPHARM analysis resulted in area under the curve, sensitivity, specificity, and balanced accuracy values of 0.94 (95% confidence interval [CI]: 0.85, 1.00), 100% (95% CI: 100, 100), 74% (95% CI: 51, 92), 87% (95% CI: 78, 98), respectively, for predicting deep MI. For predicting high-grade tumor histology, the corresponding values for the same diagnostic metrics were 0.81 (95% CI: 0.64, 0.90), 93% (95% CI: 67, 100), 63% (95% CI: 45, 79) and 78% (95% CI: 64, 86). The corresponding values achieved via radiomics were 0.92 (95% CI: 0.82, 0.95), 82% (95% CI: 65, 93), 80% (95% CI: 51, 94), 81% (95% CI: 70, 91) for deep MI and 0.72 (95% CI: 0.58, 0.83), 93% (95% CI: 65, 100), 55% (95% CI: 41, 69), 74% (95% CI: 52, 88) for high-grade histology. The diagnostic performance of the SPHARM analysis was not significantly different (P = 0.62) from that of radiomics for predicting deep MI but was significantly higher (P = 0.044) for predicting high-grade histology.

Abbreviations: 2D, Two-dimensional; 3D, Three-dimensional; ADC, Apparent diffusion coefficient; AUC, Area under receiver operating characteristics curve; CI, Confidence interval; CNN, Convolutional neural network; DCE, Dynamic contrast-enhanced; DWI, Diffusion-weighted imaging; FIGO, International Federation of Gynecology and Obstetrics; IBSI, International Biomarker Standardization Initiative; MI, Myometrial invasion; mpMRI, Multiparametric magnetic resonance imaging; MRI, Magnetic resonance imaging; RF, Random forest; ROC, Receiver operating characteristics; SPHARM, Spherical harmonics; T2WI, T2-weighted imaging; VOI, Volume of interest

* Corresponding author.
E-mail address: petersv@cim.mcgill.ca (P. Savadjiev).

[1] Peter Savadjiev and Caroline Reinhold are co-senior authors and contributed equally to this work.

https://doi.org/10.1016/j.diii.2022.10.007

Conclusion: The proposed SPHARM analysis yields similar or higher diagnostic performance than radiomics in identifying deep MI and high-grade status in histology-proven endometrial carcinoma.

1. Introduction

Magnetic resonance imaging (MRI) is an important diagnostic tool for endometrial carcinoma, the most common gynecological cancer in developed countries [1,2]. Automated analyses of MRI images using volumetry or radiomics have focused on diagnosing histopathological outcomes of endometrial carcinoma, such as high-grade status, or deep myometrial invasion (MI), from single or multiple MRI sequence (s) [3–7]. These outcomes are among those forming the basis of the International Federation of Gynecology and Obstetrics (FIGO) staging system for endometrial cancer [8]. However, after more than a decade of intensive research, it has become clear that concerns about robustness, reproducibility and standardization represent major challenges for radiomics. To address these issues, the recently formed International Biomarker Standardization Initiative (IBSI) has released recommendations for standardizing radiomic features and assessing their reproducibility [9]. Following these guidelines, an IBSI-compliant radiomic model for predicting histopathology outcomes in multiparametric MRI of endometrial cancer was recently proposed and validated on an external independent testing cohort [10].

Despite recent progress culminating in the IBSI guidelines, radiomics still faces methodological challenges. IBSI standardization requires elaborate image preprocessing, which adds significant complexity. Furthermore, radiomic features integrate information across the entire extent of the tumor, thus losing localized information which may be important for understanding which aspects of the tumor are most predictive [11]. Finally, radiomic features depend on precise segmentation of the tumor, which may take an expert radiologist a prohibitive amount of time to create, limiting the clinical applicability of this approach.

In this study, we introduced a novel machine learning framework that can address these important challenges. It builds upon standard concepts from physics and signal processing to form a robust and rotationally-invariant signature of three-dimensional (3D) image intensity data. The central idea is to perform a space/frequency decomposition of volumes of interest (VOI) in 3D image data. This decomposition is performed along a spatial dimension and an angular frequency dimension, using spherical harmonic (SPHARM) functions computed on concentric spherical shells with varying radii sampling the spatial extent of the VOI [12,13]. This approach results in a compact two dimensional (2D) descriptor for 3D image data [12] and has previously been used to represent 3D signals in a variety of domains, including astrophysics [14,15], molecular chemistry [16], evolutionary biology [17], acoustics [18], and neuroimaging [19–22]. In the present work, we theorized that SPHARM decomposition is well suited for characterizing the harmonic frequency content of solid tumors and therefore their textural appearance. To our knowledge, this is the first time such a descriptor is proposed as a quantitative radiological biomarker within a machine learning pipeline in cancer imaging. Because it computes frequency information from the image data, as opposed to directly analyzing image intensity, it does not need extensive image preprocessing and standardization as required in radiomics approaches. In addition, the proposed method allows for localization in a space/frequency domain of the most discriminative components of the predictive model. Perhaps most importantly, this method may not rely as much on a precise and time-consuming tumor segmentation as traditional radiomics, as demonstrated below with experiments comparing model performance when using precise tumor segmentations *vs.* spherical VOIs centered on the tumor which take only seconds to create.

Because of all these design choices, our main hypothesis is that a machine learning pipeline based on SPHARM descriptors will perform better than a state-of-the-art radiomics pipeline for predicting histopathological outcomes in endometrial carcinoma on MRI, specifically, the presence of deep MI and tumor high grade.

The purpose of this study was twofold: (*i*), to present the mathematical development of the SPHARM descriptor and the associated machine learning pipeline; and (*ii*), to evaluate our main hypothesis, *i.e.*, to evaluate the diagnostic performance of SPHARM descriptors and compare it to the performance of an IBSI-compliant radiomics pipeline for predicting deep MI and histopathological high-grade in preoperative multiparametric MRI.

2. Patients and methods

2.1. Patient characteristics

Institutional review board approval and waiver of informed consent were obtained for this dual-center retrospective analysis. Clinical and MRI data of women who underwent MRI before surgery between January 2011 and July 2015 were obtained from two independent institutions in two different countries, McGill University Health Centre, Montreal, Canada (Institution 1), and Hôpital Lariboisière, Assistance Publique-Hôpitaux de Paris, Paris, France (Institution 2). Data from patients recruited at the first institution (training set) were used to train the SPHARM predictive models. Their performance was validated on independent data from the second institution (validation set).

Fig. 1 presents a flowchart that summarizes the patient inclusion/exclusion criteria. These criteria are identical to those previously reported elsewhere [10], with one exception: the present study increased the minimum tumor diameter from 1 cm as used in [10] to 2.5 cm. Patients with tumor diameter below 2.5 cm were thus excluded from the present study. This increase in minumum tumor diameter was motivated by computational considerations relating to the SPHARM descriptor. It resulted in the additional exclusion of 19 women from the training set and 10 women from the validation set relative to the population sample described in [10]. Thus, in the present study, the final sample of the training set included 75 women (mean age: 65.4 ± 10.2 (standard deviation [SD]) years; range:

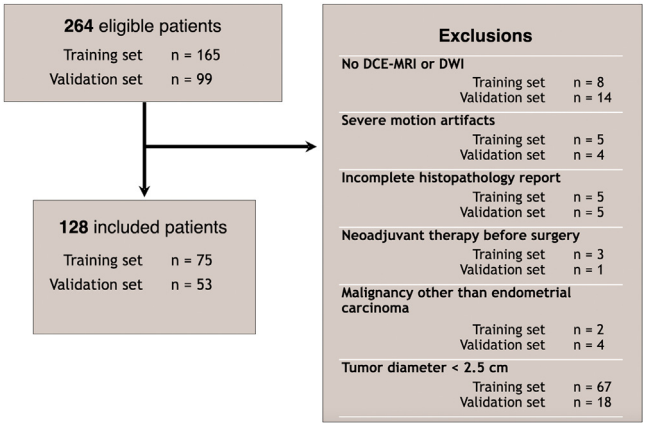

Fig. 1. Flowchart of patient selection in women with endometrial carcinoma recruited at both institutions. MI = Myometrial invasion; DCE-MRI = Dynamic contrast-enhanced magnetic resonance imaging; DWI = Diffusion-weighted imaging.

Table 1
Surgical and histopathological findings in the included sample of 128 women with endometrial carcinoma.

Variable	Training set, Institution 1 (n = 75)	Validation set, Institution 2 (n = 53)	*P* value
Age (years)	65.4 ± 10.2 [44–90]	67.0 ±11.6 [44–88]	0.57
FIGO staging			0.51
I	47 (63%)	28 (53%)	
II	3 (4%)	11 (21%)	
III	24 (32%)	10 (19%)	
IV	1 (1%)	4 (7%)	
Deep myometrial invasion			0.20
Superficial (< 50%) myometrial invasion	37 (49%)	20 (38%)	
Deep (≥ 50%) myometrial invasion	38 (51%)	33 (62%)	
Histopathological grade			0.36
Low (FIGO grade 1 and 2)	48 (64%)	38 (72%)	
High (FIGO grade 3 and non-endometrioid)	27 (36%)	15 (28%)	

Quantitative variables are expressed as means standard deviations; numbers in brackets are ranges.
Qualitative variables are expressed as raw numbers; numbers in parentheses are percentages.
FIGO = International Federation of Gynecology and Obstetrics.

44–90 years). Among them, 38 (51%) had deep MI, and 27 (36%) had high-grade tumors as assessed by histology. The final validation set in the present study included 53 women (67.0 ± 11.6 [SD] years; age range: 44–88 years). Among them, 33 (62%) had deep MI and 15 (28%) had a high-grade tumor as assessed by histology (Table 1).

2.2. MRI examinations

MRI examinations were performed on 1.5 T scanner (training set: Signa Excite; General Electric [GE] Healthcare; validation set: Magnetom® Avanto, Siemens Healthineers) using the vendor specific phased-array pelvic surface coils. MRI examinations included the following standard-of-care diagnostic sequences for pelvic MRI contrasts: fast spin echo T2-weighted imaging, echo planar imaging diffusion-weighted imaging (DWI) at b = 0 and 1000 s/mm^2, and 3D gradient echo T1-weighted dynamic contrast-enhanced (DCE)-MRI. Administration of 0.1 mmol of a gadolinium-based contrast agent per kilogram of body weight was performed intravenously prior to DCE-MRI. DCE-MRI acquisitions were obtained in the sagittal plane before contrast material administration and at three phases (time points) after administration: 25, 60, and 120 seconds after contrast material administration. In addition, images were acquired in the axial oblique plane during a delayed phase at 240 seconds after contrast material administration. In this study, the pre-contrast and the first phase of DCE-MRI were not used. We only worked with the remaining three DCE-MRI contrasts, namely, the second phase (60 s), the third phase (120 s) and the delayed phase (240 s). The MRI protocols used in each institution are summarized in Table 2. Fig. 2 illustrates an example tumor with the different MRI contrasts included in our study.

2.3. Histopathological analysis

Histological outcomes including the depth of MI (<50% *vs.* ≥50%) and tumor grade (low grade: FIGO grades 1 and 2 *vs.* high grade: FIGO grade 3 and nonendometrioid histologies) were determined using standard criteria by experienced pathologists from the surgical hysterectomy specimen as part of each patient's standard of care.

2.4. Computational methods overview

Our computational methods were based upon the creation of a 2D descriptor (matrix of SPHARM coefficients) that encoded a 2D space/frequency decomposition of the 3D image signal over a tumor VOI. This representation was compact, robust to signal noise and rotationally-invariant, that is, the representation remained the same regardless of the spatial orientation of the tumor. To perform classification on such SPHARM descriptors, a regularized tensor logistic regression (TensorReg MATLAB toolbox, version 1.0; https://hua-zhou.github.io/TensorReg/) technique was selected [23]. The logistic regression model was trained on VOIs extracted from precise manual tumor segmentations. Its diagnostic performance was evaluated using both precise tumor segmentations, as well as segmentations that consist of simple spheres centered on the tumor. Fig. 3 shows an example of precise and spherical tumor segmentations. Fig. 4 presents a visual summary of our SPHARM methods.

For comparison, we reproduced the IBSI-compliant radiomics pipeline reported previously [10]. We also computed tumor volume from precise tumor segmentations, which we then used to perform volumetry-based classification of each histopathological feature. Fig. 5 presents a visual summary of the radiomics pipeline. Full methodological details on our computational pipelines, including the SPHARM descriptors and the radiomics pipeline are presented in the Supplementary Materials, Appendices A1-A4.

2.5. Statistical analyses

Statistical analyses were performed in MATLAB (v2020b, MathWorks). Quantitative variables were expressed as means ± standard deviations (SD) and ranges. Qualitative variables were expressed as raw numbers and percentages. Receiver operating characteristic (ROC) curves and diagnostic performance metrics for the threshold maximizing Youden's index were reported (*i.e.*, sensitivity, specificity, balanced accuracy, positive and negative predictive values) along with their bootstrapped 95% confidence intervals (CI). Paired ROC curves were compared with a DeLong test with Bonferroni-Holm correction for multiple comparisons in R (v3.6.2, R Foundation) [24].

2.6. Implementation

Our code is publicly available at: https://github.com/thierleft/3Dspharm-decomposition-tumor.

3. Results

3.1. Predicting deep myometrial invasion

Both the SPHARM and radiomics methods achieved non-significantly different performances on the validation set for predicting deep MI based on features extracted from all MRI contrasts (AUC of 0.94 [95% CI: 0.85, 1.00] vs. 0.92 [95% CI: 0.82, 0.95]; P = 0.62) (Table 3). The coefficients of the logistic regression model combining SPHARM predictions from individual MRI sequences obtained on the training set are shown in Table 4. SPHARM performed robustly from training to validation with consistent AUC and balanced accuracy

Table 2
Pelvic MRI protocols at institution 1 and at institution 2.

MRI scanner	Image type	Sequence	Acquisition plane	TR/TE (ms)	FOV (cm)	Section thickness (mm)	*b*-value (s/mm^2)
1.5-T GE Signa1 Excite	T2WI	FSE	Sagittal, Axial-oblique*	4000-4575/100	24	4	N.A.
(Institution 1, Training set)	DWI	EPI	Sagittal, Axial-oblique*	5000/69	32	6	0, 1000
	DCE-T1WI	3D-GRE	Sagittal, Axial-oblique*	3.6/1.75	26	4	N.A.
1.5-T Siemens Avanto	T2WI	FSE	Sagittal, Axial oblique*	3920-7660/144-147	18-30	3-4	N.A.
(Institution 2, Validation set)	DWI	EPI	Axial-oblique*	3000/91	38	5	0, 1000
	DCE-T1WI	3D-GRE	Sagittal, Axial-oblique*	5.43/2.5	25	1.8	N.A.

3D-GRE= Three-dimensional gradient-echo; DCE = Dynamic contrast-enhanced; DWI = Diffusion-weighted imaging; EPI = Echo planar imaging; FOV= Field of view; FSE = Fast spin-echo; N.A. = Not applicable; T1WI = T1-weighted imaging; T2WI = T2-weighted imaging; TE = Echo time; TR = Repetition time. *The axial-oblique plane was perpendicular to the endometrial cavity, resulting in a short-axis view.

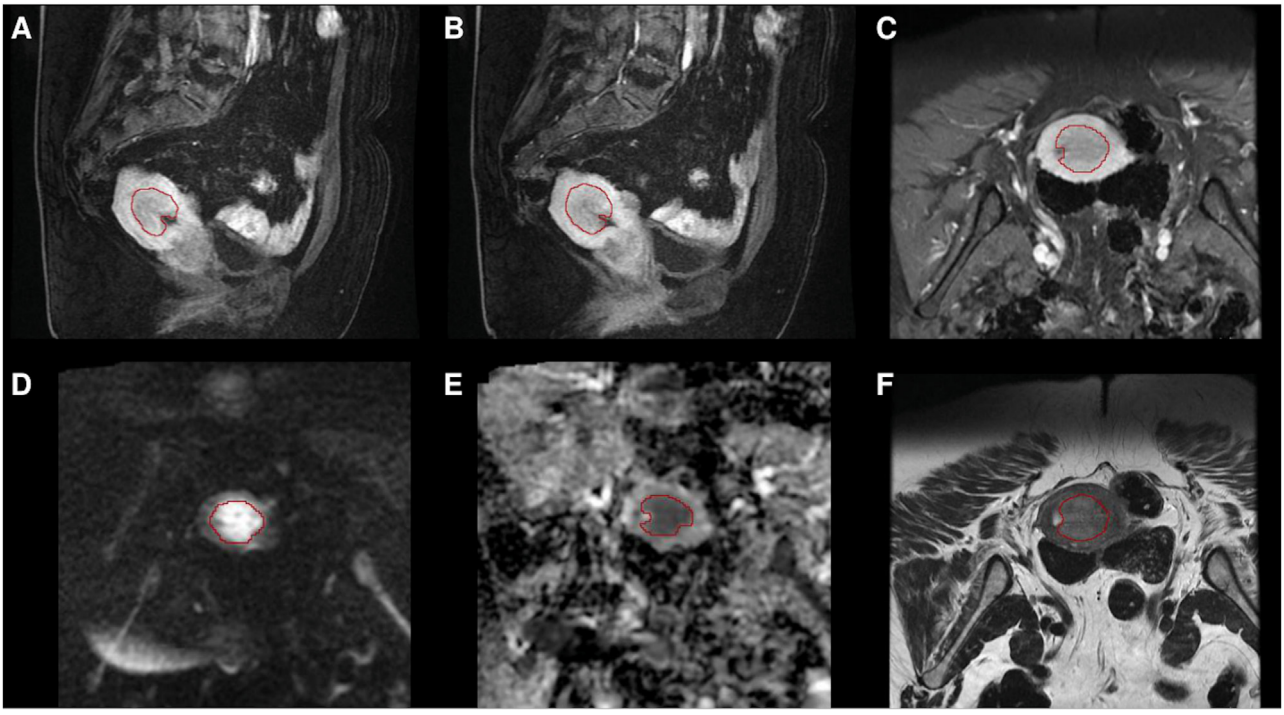

Fig. 2. Segmented endometrial tumor with International Federation of Gynecology and Obstetrics (FIGO) stage IIIC1 in an 80-year-old woman on (A) sagittal second-phase dynamic contrast-enhanced magnetic resonance imaging (DCE-MRI) (60 s), (B) third-phase DCE-MRI (120 s), (C) axial oblique delayed-phase DCE-MRI (240 s), (D) DWI (b = 1000 s/mm^2), (E) Apparent diffusion coefficient map, and (F) T2-weighted imaging. The manually measured maximal diameter was 40 mm and deep myometrial invasion was observed at MRI. Histopathological analysis confirmed the presence of deep myometrial invasion and of a high-grade tumor (grade 3). Segmented contours are shown in red.

values. To confirm that SPHARM predictions were not capturing only tumor volume, the diagnostic performance of MRI volumetry was also reported for the classification of deep MI, resulting in a significantly lower performance with volumetry on the validation set (AUC of 0.94 [95% CI: 0.85, 1.00] for SPHARM *vs.* 0.77 [95% CI: 0.60, 0.86] for volumetry; $P = 0.034$) (Table 3).

Based on the associated logistic regression coefficients on the SPHARM predictions extracted from each MRI sequence (Table 4), the most relevant MRI contrasts were ADC maps and the second phase (at 60 s) DCE-MRI. Because of this, and also based on the knowledge that both ADC maps and DCE-MRI can be highly predictive of the depth of MI quantitatively and visually [25], we analyzed the diagnostic performance of radiomics and SPHARM only on the ADC maps, and only on second phase (60 s) DCE-MRI (Table 3). On these individual contrasts, SPHARM provided statistically significant improvements over radiomics on the validation set on second phase DCE-MRI (AUC of 0.86 [95% CI: 0.63, 0.96] *vs.* 0.68 [95% CI: 0.53, 0.81]; $P = 0.032$). The improvement over radiomics on ADC was not statistically significant (AUC of 0.85 [95% CI: 0.71, 0.94] *vs.* 0.76 [95% CI: 0.65, 0.84]; $P = 0.12$). The ROC curves for performance on ADC and second phase DCE-MRI, as well as TensorReg classification matrices of SPHARM descriptors of both MRI contrasts, are presented in Figs. 6 and 7. Additional discussion on these results is included in the Supplementary Materials.

3.2. Predicting high-grade status

Combining information from all MRI contrasts, SPHARM outperformed radiomics in identifying high-grade status at histopathological examination (validation AUC of 0.81 [95% CI: 0.64, 0.90] *vs.* 0.72 [95% CI: 0.58, 0.83]; $P = 0.044$; Table 5). Similarly, SPHARM predictions provided increased diagnostic performance compared to that of MRI volumetry for identifying high-grade endometrial carcinoma (validation AUC of 0.81 [95% CI: 0.64, 0.90] *vs.* 0.70 [95% CI: 0.53, 0.82]; $P = 0.040$).

The most relevant MRI contrast for the prediction of the tumor grade with SPHARM decomposition retrieved from tensor logistic regression was delayed phase DCE-MRI as seen in Table 4. Based on this, the diagnostic performance of radiomics and SPHARM was analyzed only on the delayed DCE phase (Table 5). SPHARM maintained a higher performance compared to radiomics, which dropped down to nearly random performance (validation AUC of 0.79 [95% CI: 0.62, 0.94] *vs.* 0.51 [95% CI: 0.36, 0.70]; $P = 0.012$). The ROC curve for performance on the delayed phase of DCE-MRI and the corresponding

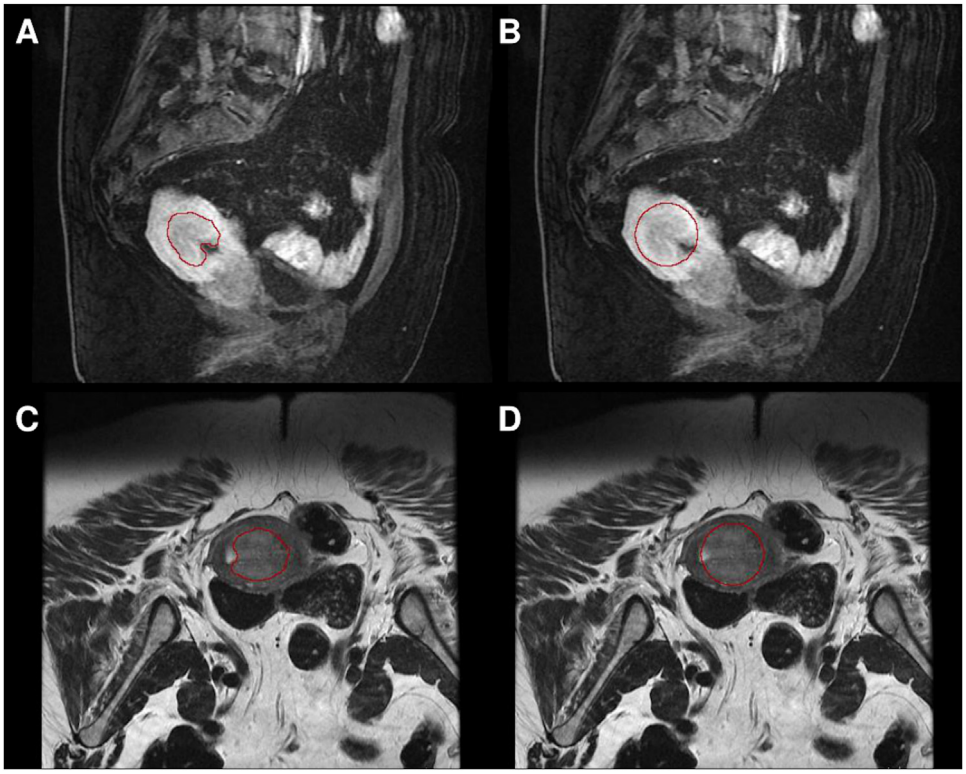

Fig. 3. Representative segmented endometrial carcinoma on third-phase (120 s) dynamic contrast-enhanced magnetic resonance imaging (A) with precise manual contouring and (B) with a spherical volume of interest, and on T2-weighted imaging (C) with precise manual contouring and (D) with a spherical volume of interest. Segmented contours are shown in red.

TensorReg classification matrix are presented in Fig. 8. Additional discussion on these results is included in the Supplementary Materials.

3.3. Analyses with spherical volumes of interest

Applying the SPHARM model to spherical VOIs produced a performance that was stable and robust, yielding similar AUC values across training and validation sets for predicting both deep MI and high grade (Table 6). By contrast, when radiomics was applied with the full spherical VOIs, there was a substantial drop in performance between training and validation AUC for both outcomes. Second, while both SPHARM and radiomics resulted in decreased performance for predicting deep MI when going from precisely segmented to spherical VOIs (SPHARM: validation AUC of 0.94 [95% CI: 0.85, 1.00] *vs.* 0.80 [95% CI: 0.47, 0.97]; P =0.039; radiomics: validation AUC of 0.92 [95% CI: 0.81, 0.98] *vs.* 0.69 [95% CI: 0.50, 0.77]; P = 0.022) the decrease was much less pronounced for SPHARM than for radiomics. Finally, while the validation AUC of radiomics for predicting high-grade decreased to being essentially random when moving from precise to spherical VOIs (0.72 [95% CI: 0.58, 0.83] *vs.* 0.52 [95% CI: 0.34, 0.67]; P = 0.028), the validation AUC of SPHARM increased not significantly from 0.81 [95% CI: 0.64, 0.90] to 0.87 [95% CI: 0.76, 0.97] (P = 0.069).

Fig. 9 presents the ROC curves for diagnostic performance of SPHARM descriptors on spherical VOIs and on precise VOIs, for the case of the diagnostic model combining all MRI contrasts.

4. Discussion

This study introduces SPHARM-based diagnostic models for assessing histopathological features of endometrial cancer on mpMRI. However, the same methodology could have potential applications in many other cancer types.

Our comparison point was a radiomics analysis that follows current IBSI recommendations for reproducibility and robustness [9,10]. In addition to radiomics, recent years have seen a tremendous increase in interest in convolutional neural networks (CNN), a type of deep learning model specifically designed for image analysis [26]. However, applications of CNNs specifically to MRI of endometrial cancer have been relatively scarce.

A recent CNN-based study reported an AUC of 0.78 and a balanced accuracy (mean of sensitivity and specificity) of 77% for the detection of deep myometrial invasion on T2-weighted MR images [27]. One limitation of this study is that it is based on a single patient cohort from a single institution [27]. This CNN model's performance validated on data from a single institution is lower than our SPHARM model's performance validated on data from an independent institution, even when we used single MRI contrasts (ADC or second phase DCE-MRI at 60 s), and also when we used spherical VOIs with all MRI contrasts. In another single-center study, a CNN-based approach was applied to 72 patients diagnosed with surgico-pathological stage I endometrial carcinoma to classify them based on myometrial invasion into stage IA or IB, achieving an accuracy of 79.2% [28]. Another study used CNNs to distinguish cancerous from non-cancerous endometrial lesions [29].

In the present work, we did not compare our results to a CNN approach. However, the rotational invariance of our SPHARM signature and its sensitivity to frequency (as opposed to intensity) naturally obviates the need for some data augmentation steps that would have been required in a CNN-based approach. Unlike a CNN model, our tensor logistic regression model based on SPHARM descriptors is compact and interpretable, and does not require transfer learning or data augmentation heuristics.

Compared to an IBSI-compliant radiomics pipeline, the SPHARM method presents theoretical and practical advantages. First, since it captures image frequency as opposed to intensity, it avoids several preprocessing steps associated with radiomics, for instance signal

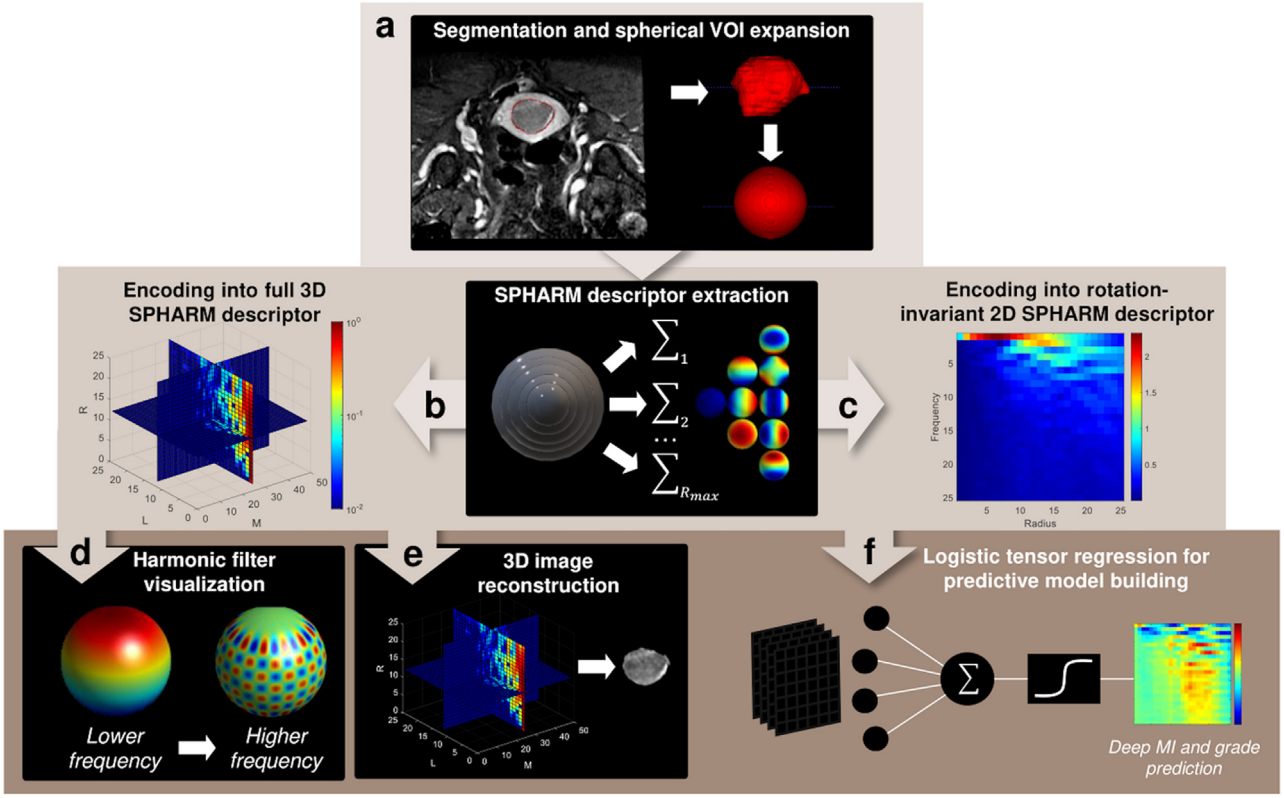

Fig. 4. Schematic illustration of the spherical harmonic (SPHARM) decomposition workflow developed for unravelling histopathological phenotypes of endometrial carcinoma on multiparametric magnetic resonance imaging (MRI). (A) After manual segmentation, the three-dimensional (3D) volume of interest is extracted as such, or is expanded to a 3D sphere, both for SPHARM decomposition. Radially equidistant shells are used to sample the tumor region in spherical coordinates. Expansion of SPHARM coefficients is obtained for each sampled shell to build either (B) a full 3D SPHARM descriptor which allows image reconstruction and harmonic filter visualization, or (C) as a two-dimensional (2D) rotationally-invariant SPHARM descriptor for the purposes of predictive model building. (D) Individual coefficients in a SPHARM descriptor can be singled out based on their predictive importance, and an associated harmonic filter can be visualized from the 3D SPHARM descriptor, or (E) the full descriptor can be used to reconstruct the original image via an inverse transform from this compact representation with minimal image distortion. (F) The 2D SPHARM descriptors were used for classification of deep myometrial invasion and high-grade status endometrial carcinoma on MRI after training a regularized logistic tensor regression classifier on the training set and applying it on the validation set. Continuous risks for each endpoint were obtained by taking the inner scalar product of 2D SPHARM descriptors and the resulting 2D classification matrices.

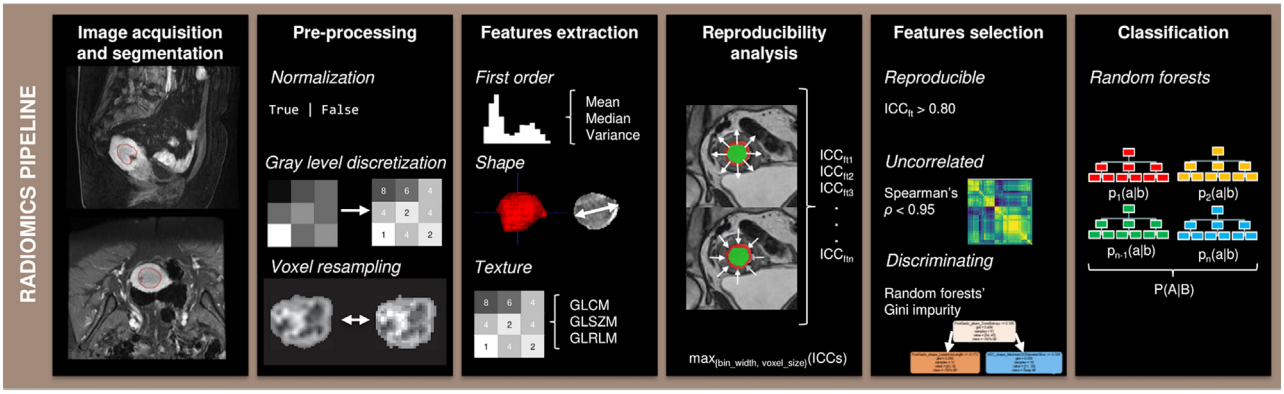

Fig. 5. Radiomics pipeline developed for the classification of histopathological features of endometrial carcinoma on magnetic resonance imaging (MRI), as previously described [10]. After manual segmentation of the tumor, radiomics features are extracted for different sets of preprocessing parameters and the set leading to the highest feature stability under volume of interest variations is selected. Only preselected reproducible, uncorrelated and discriminating radiomics features across all MRI contrasts are included into the final random forest classification. Random forest models are trained on the training set and diagnostic performance is reported on both training and validation sets. Figure adapted from [10].

discretization in bins. Furthermore, typical radiomics pipelines include a feature selection step prior to classification [30]. Such a step may hinder reproducibility as it usually involves a choice of an arbitrary threshold on a selection criterion that ultimately decides which features to include in the final model. Furthermore, this selection is not accounted for in the uncertainty estimates of the final model. In contrast, the proposed SPHARM method does not involve such a feature selection step. In terms of absolute performance, as well as in terms of consistency of performance across training and validation sets, SPHARM did at least as well or better than the IBSI-based radiomics pipeline in our experiments, despite the lack of strict preprocessing, standardization and feature selection prior to classification.

The space-frequency decomposition in SPHARM allows for spatial localization of discriminative regions in a tumor to spherical shells with certain radii and/or to certain bands of angular frequencies. In addition to being potentially informative about tumor biology and/or

Table 3
Detailed diagnostic performance of radiomics and SPHARM pipelines for predicting deep myometrial invasion.

Deep myometrial invasion		AUC	Sensitivity (%)	Specificity (%)	Balanced accuracy (%)	PPV (%)	NPV (%)	*P* value (Validation)*
All MRI contrasts	SPHARM, Training	0.94 (0.85, 0.98)	82 (68, 93)	93(73, 100)	88 (77, 94)	93 (78, 100)	82 (64, 92)	0.620
	SPHARM, Validation	**0.94 (0.85, 1.00)**	**100 (100, 100)**	**74 (51, 92)**	**87 (78, 98)**	**88 (71, 98)**	**100 (100, 100)**	
	Radiomics, Training	0.92 (0.82, 0.95)	93 (82, 98)	75 (62, 85)	82 (75, 90)	74 (60, 85)	94 (82, 98)	
	Radiomics, Validation	0.92 (0.81, 0.98)	82 (65, 93)	80 (51, 94)	81 (70, 91)	89 (70, 97)	72 (55, 91)	
ADC maps only	SPHARM, Training	0.91 (0.81, 0.97)	75 (56, 87)	93 (77, 100)	82 (71, 90)	93 (74, 100)	74 (56, 87)	0.120
	SPHARM, Validation	**0.85 (0.71, 0.94)**	**62 (43, 80)**	**93 (70, 100)**	**78 (62, 88)**	**94 (65, 100)**	**60 (41, 76)**	
	Radiomics, Training	0.77 (0.63, 0.88)	74 (61, 87)	72 (59, 86)	74 (61, 86)	67 (63, 71)	79 (70, 87)	
	Radiomics, Validation	0.76 (0.65, 0.84)	92 (78, 98)	52 (35, 72)	74 (61, 84)	72 (58, 84)	82 (58, 100)	
Second phase DCE-MRI only	SPHARM, Training	0.87 (0.77, 0.94)	67 (51, 83)	90 (72, 97)	79 (64, 86)	87 (65, 96)	71 (54, 84)	0.032
	SPHARM, Validation	**0.86 (0.63, 0.96)**	**95 (73, 100)**	**58 (30, 86)**	**82 (65, 94)**	**81 (63, 96)**	**88 (40, 100)**	
	Radiomics, Training	0.70 (0.54, 0.82)	86 (68, 100)	55 (40, 72)	71 (60, 81)	60 (54, 64)	85 (67, 100)	
	Radiomics, Validation	0.68 (0.53, 0.81)	70 (50, 82)	60 (40, 76)	65 (53, 75)	70 (53, 82)	59 (41,78)	
MRI volumetry reference (T2WI)	Training	0.58 (0.44, 0.71)	28 (14, 42)	93 (79, 100)	60 (44, 67)	85 (50, 100)	58 (35, 62)	0.034
	Validation	0.77 (0.60, 0.86)	59 (42, 75)	86 (76, 98)	73 (62, 81)	86 (66, 96)	59 (42, 76)	

Data in parentheses are bootstrapped 95% confidence intervals. * DeLong test comparing the ROC curve between SPHARM analysis and radiomics analysis performed in the validation set with the given MRI contrast(s). In the case of MRI volumetry, the DeLong test compares the ROC curve for SPHARM analysis on all MRI contrasts and MRI volumetry in the validation set. AUC = Area under the receiver operating characteristic curve; PPV = Positive predictive value; NPV = Negative predictive value; MRI = Magnetic resonance imaging; SPHARM = Spherical harmonics; ADC = Apparent diffusion coefficient; DCE-MRI = Dynamic contrast-enhanced magnetic resonance imaging; T2WI = T2-weighted imaging.

Table 4
Logistic regression coefficients obtained for each MRI contrast for identifying deep myometrial invasion and high grade from TensorReg predictions on SPHARM decomposition of images.

Histological feature	MRI sequence	Estimated logistic regression coefficients	Bootstrapped standard deviation
Deep myometrial invasion	ADC	1.92	0.62
	DWI	0.01	0.21
	T2WI	0.47	0.29
	Second-phase DCE-MRI	2.12	1.02
	Third-phase DCE-MRI	0.75	0.35
	Delayed-phase DCE-MRI	0.47	0.30
High grade	ADC	1.25	0.32
	DWI	0.01	0.04
	T2WI	0.51	0.15
	Second-phase DCE-MRI	0.71	0.19
	Third-phase DCE-MRI	1.22	0.26
	Delayed-phase DCE-MRI	2.03	0.93

ADC = Apparent diffusion coefficient; DCE = Dynamic contrast-enhanced; DWI = Diffusion-weighted imaging; MRI = Magnetic resonance imaging; T2WI = T2-weighted imaging.

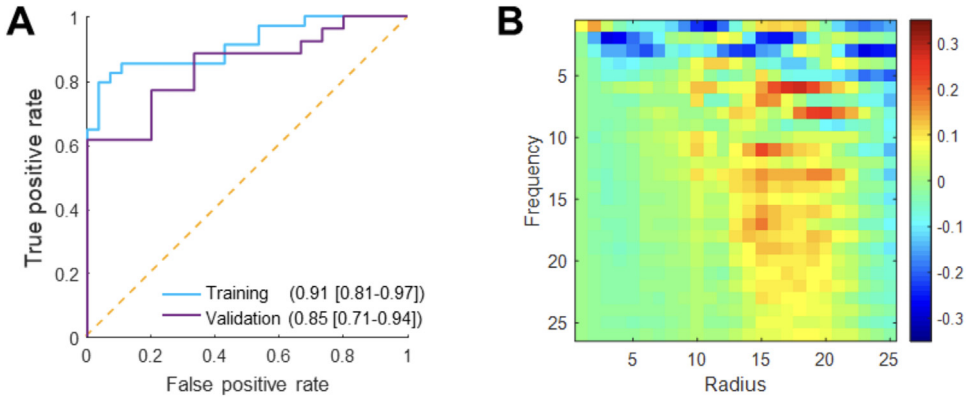

Fig. 6. (A) Training and validation receiver operating characteristics (ROC) curves with area under receiver operating characteristics curve (AUC) values for predicting deep myometrial invasion with spherical harmonic (SPHARM) descriptors on apparent diffusion coefficient maps, and (B) classification matrix obtained by tensor logistic regression trained on SPHARM descriptors.

radiological appearance properties, this localization may also be key to understanding why spherical VOIs perform better at predicting certain outcomes. In fact, a general understanding of the conditions that ensure the success of spherical VOIs is important for the ability to plan whether to invest time and efforts in precisely contouring the validation data, or whether simple spherical VOIs might suffice. A rigorous answer to these important questions is beyond the scope of the present study and will be the topic of a future work. However, we present in the Supplementary Materials additional results to provide some initial answers, and to suggest a roadmap for a more systematic future investigation. These preliminary results indicate that indeed, the space-frequency localization properties of the classification matrix are important for understanding the performance of spherical VOIs on our data.

The main limitation of the SPHARM method is that it can only work with tumors larger than some minimum size, in order to ensure

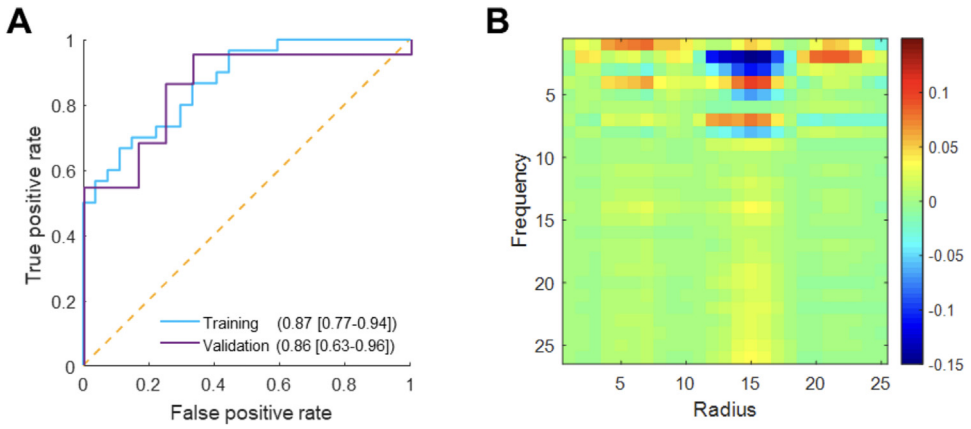

Fig. 7. (A) Training and validation receiver operating characteristics (ROC) curves with area under receiver operating characteristics curve (AUC) values for predicting deep myometrial invasion with spherical harmonic (SPHARM) descriptors on second-phase dynamic contrast-enhanced magnetic resonance imaging, and (B) classification matrix obtained by tensor logistic regression.

Table 5
Detailed diagnostic performance of radiomics and SPHARM pipelines for predicting high-grade endometrial cancer.

High grade		AUC	Sensitivity (%)	Specificity (%)	Balanced accuracy (%)	PPV (%)	NPV (%)	*P* value (Validation)*
All MRI contrasts	SPHARM, Training	0.89 (0.76, 0.96)	92 (74, 100)	82 (67, 92)	86 (75, 92)	76 (59, 90)	82 (64, 92)	0.044
	SPHARM, Validation	**0.81 (0.64, 0.90)**	**93 (67, 100)**	**63 (45, 79)**	**78 (64, 86)**	**58 (37, 86)**	**95 (68, 100)**	
	Radiomics, Training	0.79 (0.72, 0.88)	90 (76, 97)	68 (56, 79)	76 (68, 86)	60 (48, 75)	94 (83, 98)	
	Radiomics, Validation	0.72 (0.58, 0.83)	93 (65, 100)	55 (41, 69)	74 (52, 88)	41 (25, 58)	96 (80, 100)	
Delayed phase DCE-MRI only	SPHARM, Training	0.77 (0.62, 0.88)	91 (68, 100)	58 (45, 76)	74 (64, 84)	58 (44, 76)	91 (70, 100)	0.012
	SPHARM, Validation	**0.79 (0.62, 0.94)**	**82 (55, 100)**	**68 (54, 84)**	**75 (65, 86)**	**59 (45, 77)**	**89 (66, 98)**	
	Radiomics, Training	0.61 (0.49, 0.77)	58 (40, 74)	69 (58, 81)	64 (49, 78)	47 (33, 64)	74 (65, 85)	
	Radiomics, Validation	0.51 (0.36, 0.70)	31 (10, 56)	79 (60, 97)	53 (38, 72)	43 (14, 80)	72 (58, 93)	
MRI volumetry reference (T2WI)	Training	0.57 (0.44, 0.71)	67 (48, 82)	55 (42, 71)	61 (47, 70)	47 (32, 64)	73 (56, 87)	0.040
	Validation	0.70 (0.53, 0.82)	67 (43, 87)	77 (63, 88)	72 (61,83)	53 (30, 75)	86 (70, 94)	

Data in parentheses are bootstrapped 95% confidence intervals. * DeLong test comparing the ROC curve between SPHARM analysis and radiomics analysis performed in the validation set with the given MRI contrast(s). In the case of MRI volumetry, the DeLong test compared the ROC curve for SPHARM analysis on all MRI contrasts and MRI volumetry in the validation set. ADC = Apparent diffusion coefficient; AUC = Area under the receiver operating characteristic curve; DCE-MRI = Dynamic contrast-enhanced magnetic resonance imaging; MRI = Magnetic resonance imaging; NPV = Negative predictive value; PPV = Positive predictive value; SPHARM = Spherical harmonics; T2WI = T2-weighted imaging.

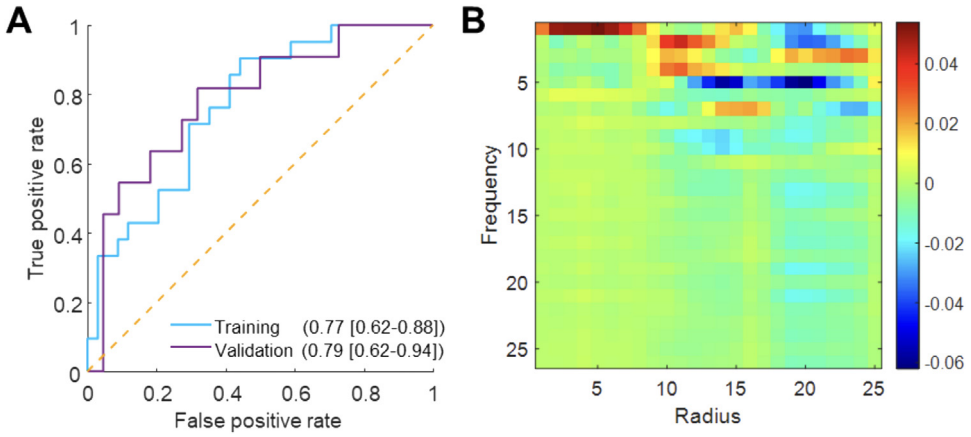

Fig. 8. (A) Training and validation receiver operating characteristics (ROC) curves with area under receiver operating characteristics curve (AUC) values for differentiating low from high grade endometrial cancer with spherical harmonic (SPHARM) descriptors on delayed-phase dynamic contrast-enhanced magnetic resonance imaging, and (B) classification matrix obtained by tensor logistic regression.

a signal with a sufficient spatial extent needed to compute SPHARM descriptors in a meaningful way. This minimum size, 2.5 cm in the present study, is larger than the tumor diameter threshold of 1 cm typically used in radiomics studies, for instance as in Lefebvre et al. study [10]. Nevertheless, compared to the sample size used in Lefebvre et al. study [10], only a relatively small number of additional lesions had to be excluded in our study after increasing the minimum tumor diameter from 1 cm to 2.5 cm. Furthermore, it has previously been argued that a tumor diameter of 2.0 cm [31] or 2.8 cm [32] can be used as a threshold to predict presence or absence of deep MI. Based on this, one might have expected that exclusion of tumors with diameter <2.5 cm will remove nearly all tumors without deep MI, making the classification task unrealistically easy. This, however, is far from being true in our data. Following the exclusion of tumors with diameter <2.5 cm, there are still nearly 50% of the tumors included in our training data and 38% of those included in the

Table 6
Detailed diagnostic performance of SPHARM and radiomics pipelines for predicting deep myometrial invasion and high-grade status on multiparametric MRI in spherical tumor volumes of interest.

		AUC	Sensitivity (%)	Specificity (%)	Balanced accuracy (%)	PPV (%)	NPV (%)	*P* value (Validation)*
Deep myometrial invasion	SPHARM, Training	0.81 (0.71, 0.89)	77 (52, 93)	79 (62, 97)	79 (64, 86)	82 (64, 98)	69 (51, 84)	0.038
All MRI contrasts	**SPHARM, Validation**	**0.80 (0.47, 0.97)**	**81 (55, 94)**	**73 (45, 100)**	**78 (62, 91)**	**86 (58, 100)**	**65 (38, 90)**	
	Radiomics, Training	0.82 (0.72, 0.89)	84 (72, 93)	63 (48, 78)	75 (64, 81)	71 (58, 80)	80 (66, 91)	
	Radiomics, Validation	0.69 (0.50, 0.77)	77 (58, 92)	45 (33, 65)	63 (50, 77)	42 (25, 58)	84 (63, 94)	
High grade	SPHARM, Training	0.91 (0.86, 0.96)	82 (66, 97)	92 (81,100)	88 (76, 96)	94 (74, 100)	72 (56, 86)	<0.001
All MRI contrasts	**SPHARM, Validation**	**0.87 (0.76, 0.97)**	**72 (56, 94)**	**99 (82, 100)**	**85 (70, 99)**	**81 (55, 100)**	**78 (58, 89)**	
	Radiomics, Training	0.62 (0.49, 0.73)	88 (72, 97)	41 (31, 53)	58 (35, 68)	44 (32, 56)	87 (70, 97)	
	Radiomics, Validation	0.52 (0.34, 0.67)	80 (55, 100)	38 (26, 53)	48 (35, 61)	29 (15, 46)	85 (66, 96)	

AUC = Area under the receiver operating characteristic curve; MRI = Magnetic resonance imaging; NPV = Negative predictive value; PPV = Positive predictive value; SPHARM = Spherical harmonics. *DeLong test comparing the ROC curve between SPHARM analysis and radiomics analysis performed in the validation set with the given MRI contrast(s).

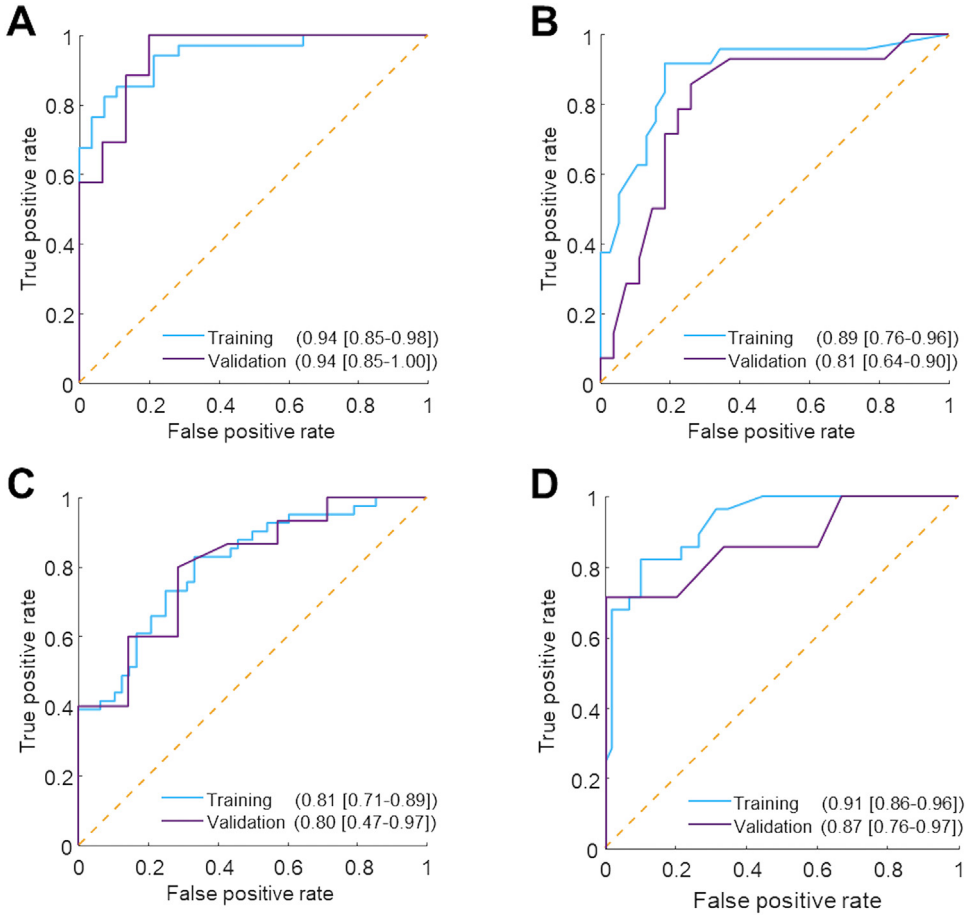

Fig. 9. Training and validation receiver operating characteristic curves for diagnostic models based on spherical harmonic (SPHARM) descriptors combining all magnetic resonance imaging sequences for predicting deep myometrial invasion from precise manual segmentations (A), for predicting high-grade endometrial cancer from precise manual segmentations (B), for predicting deep myometrial invasion from spherical volumes of interest (C), and for predicting high-grade endometrial cancer from spherical volumes of interest (D).

validation set that are without deep MI. Furthermore, as an additional indication that excluding the smallest tumors is not easing the prediction task, we extracted the volume of the remaining tumors and computed its diagnostic performance, achieving poor results in classifying both histopathological features. Another limitation stems from machine learning considerations. In machine learning, predictive models are trained on one set, usually split in two for training and validation, the latter being used for parameter tuning and assessment of the model's training, prior to applying it to test data. A separate and independent set is reserved for testing the model's performance in an unbiased manner. Here, we used our entire first set for training, and the second independent set for validation and for tuning a single parameter (*i.e.*, the logistic regression regularization parameter λ). As such, our results do not present a true independent testing of the model. This important step will be carried out in future work with a third independent cohort. We chose this strategy due to the small size of our training set, which makes splitting it difficult. Furthermore, while regularization parameter tuning is common in logistic regression, this is the first time that SPHARM descriptors and the TensorReg classification model are used for image-based tumor assessment. In this context, no prior knowledge exists on how to set the regularization parameter. Therefore, we wanted to ensure parameter tuning happened in an unbiased manner on an independent set. This strategy has the potential of reducing overfitting when the model is applied to other independent test sets. Finally, our current results are still informative about model performance across

independent sets, given optimal regularization settings. Finally, an apparent limitation may stem from the relatively small size of our sample. However, our sample size is similar to (or larger than) that of other radiomics or volumetry studies on histopathological outcomes in endometrial cancer [3–7]. Furthermore, we remind the reader that our two datasets come from two independent institutions in two different countries, and were acquired on scanners from two different manufacturers. Despite this, and despite the relatively small size of our training set, the algorithms and especially the SPHARM method performed robustly across these two sets.

In conclusion, we report a method for quantitative image analysis based on spherical harmonics and applied it for the first time to predict histopathological outcomes in cancer MRI. This method does not require extensive image preprocessing and standardization as in radiomics approaches. Furthermore, it allows for localization in a space/frequency domain of the most discriminative model components. Finally, this method does not appear to rely as much on precise tumor segmentations as radiomics. While the training set needs to be precisely segmented, once the trained model is available, it might be possible to apply it to new data that only has spherical segmentations. This has the potential of considerably simplifying and reducing the radiologist's and radiation oncologist's workload when employing machine learning techniques and quantitative imaging descriptors for enhanced clinical decision making.

Human rights

The authors declare that the work described has been performed in accordance with the Declaration of Helsinki of the World Medical Association revised in 2013 for experiments involving humans.

Informed consent and patient details

The institutional review board of our institutions approved this study. The authors declare that this report does not contain any personal information that could lead to the identification.

Author contributions

All authors attest that they meet the current International Committee of Medical Journal Editors (ICMJE) criteria for Authorship.

Declaration of Competing Interest

The authors of this manuscript declare no relationships with any companies, whose products or services may be related to the subject matter of the article.

CRediT authorship contribution statement

Thierry L. Lefebvre: Conceptualization, Methodology, Software, Validation, Visualization, Writing – original draft. **Ozan Ciga:** Conceptualization, Methodology. **Sahir Rai Bhatnagar:** Methodology. **Yoshiko Ueno:** Data curation. **Sameh Saif:** Data curation. **Eric Winter-Reinhold:** Data curation. **Anthony Dohan:** Resources, Data curation. **Philippe Soyer:** Resources, Supervision, Data curation. **Reza Forghani:** Writing – review & editing. **Kaleem Siddiqi:** Conceptualization. **Jan Seuntjens:** Conceptualization. **Caroline Reinhold:** Resources, Writing – review & editing, Supervision, Project administration. **Peter Savadjiev:** Conceptualization, Methodology, Validation, Visualization, Writing – review & editing, Supervision, Project administration.

Funding information

This work was jointly funded by the Fonds de recherche du Québec - Santé (FRQS) and the Fondation de l'association des radiologistes du Québec (FARQ). TLL would like to acknowledge financial support from the Natural Sciences and Engineering Research Council of Canada (NSERC) Alexander Graham Bell Canada Graduate Scholarship. K. Siddiqi and P. Savadjiev are grateful to NSERC for research support.

Supplementary materials

Supplementary material associated with this article can be found in the online version at doi:10.1016/j.diii.2022.10.007.

References

[1] Bray F, Ferlay J, Soerjomataram I, Siegel RL, Torre LA, Jemal A. Global cancer statistics 2018: GLOBOCAN estimates of incidence and mortality worldwide for 36 cancers in 185 countries. CA Cancer J Clin 2018;68:394–424.
[2] Sala E, Rockall AG, Freeman SJ, Mitchell DG, Reinhold C. The added role of MR imaging in treatment stratification of patients with gynecologic malignancies: what the radiologist needs to know. Radiology 2013;266:717–40.
[3] Ueno Y, Forghani B, Forghani R, Dohan A, Zeng XZ, Chamming's F, et al. Endometrial carcinoma: MR imaging-based texture model for preoperative risk stratification: a preliminary analysis. Radiology 2017;284:748–57.
[4] Stanzione A, Cuocolo R, Del Grosso R, Nardiello A, Romeo V, Travaglino A, et al. Deep myometrial infiltration of endometrial cancer on MRI: a radiomics-powered machine learning pilot study. Acad Radiol 2021;28:737–44.
[5] Ytre-Hauge S, Dybvik JA, Lundervold A, Salvesen OO, Krakstad C, Fasmer KE, et al. Preoperative tumor texture analysis on MRI predicts high-risk disease and reduced survival in endometrial cancer. J Magn Reson Imaging 2018;48:1637–47.
[6] Bereby-Kahane M, Dautry R, Matzner-Lober E, Cornelis F, Sebbag-Sfez D, Place V, et al. Prediction of tumor grade and lymphovascular space invasion in endometrial adenocarcinoma with MR imaging-based radiomic analysis. Diagn Interv Imaging 2020;101:401–11.
[7] Nougaret S, Reinhold C, Alsharif SS, Addley H, Arceneau J, Molinari N, et al. Endometrial cancer: combined MR volumetry and diffusion-weighted imaging for assessment of myometrial and lymphovascular invasion and tumor grade. Radiology 2015;276:797–808.
[8] Creasman W. Revised FIGO staging for carcinoma of the endometrium. Int J Gynaecol Obstet 2009;105:109.
[9] Zwanenburg A, Vallieres M, Abdalah MA, Aerts H, Andrearczyk V, Apte A, et al. The image biomarker standardization initiative: standardized quantitative radiomics for high-throughput image-based phenotyping. Radiology 2020;295:328–38.
[10] Lefebvre TL, Ueno Y, Dohan A, Chatterjee A, Vallières M, Winter-Reinhold E, et al. Development and validation of multiparametric MRI-based radiomics models for preoperative risk stratification of endometrial cancer. Radiology 2022;305:375–86.
[11] Sala E, Mema E, Himoto Y, Veeraraghavan H, Brenton JD, Snyder A, et al. Unravelling tumour heterogeneity using next-generation imaging: radiomics, radiogenomics, and habitat imaging. Clin Radiol 2017;72:3–10.
[12] Kazhdan M, Funkhouser T, Rusinkiewicz S. Rotation invariant spherical harmonic representation of 3D shape descriptors. In: Proceedings of the 2003 Eurographics/ACM SIGGRAPH symposium on Geometry processing. Eurographics Association; 2003. p. 156–64.
[13] Skibbe H, Wang Q, Ronneberger O, Burkhardt H, Reisert M. Fast computation of 3D spherical Fourier harmonic descriptors: complete orthonormal basis for a rotational invariant representation of three-dimensional objects. 2009 IEEE 12th International Conference on Computer Vision Workshops, ICCV Workshops; 2009. p. 1863–9.
[14] Abrial P, Moudden Y, Starck J-L, Afeyan B, Bobin J, Fadili J, et al. Morphological component analysis and inpainting on the sphere: application in physics and astrophysics. J Fourier Anal Appl 2007;13:729–48.
[15] Knaack R, Stenflo JO. Spherical harmonic decomposition of solar magnetic fields. Astron Astrophys 2005;438:349–63.
[16] Yoshii N, Nimura Y, Fujimoto K, Okazaki S. Spherical harmonics analysis of surface density fluctuations of spherical ionic SDS and nonionic C12E8 micelles: a molecular dynamics study. J Chem Phys 2017;147:034906.
[17] Shen L, Farid H, McPeek MA. Modeling three-dimensional morphological structures using spherical harmonics. Evolution 2009;63:1003–16.
[18] Zotter F, Frank M. Ambisonic amplitude panning and decoding in higher orders: a practical 3D audio theory for recording, studio production, sound reinforcement, and virtual reality. Cham: Springer International Publishing; 2019. p. 53–98.
[19] Galinsky VL, Frank LR. Automated segmentation and shape characterization of volumetric data. Neuroimage 2014;92:156–68.
[20] Kainz B, Keraudren K, Kyriakopoulou V, Rutherford M, Hajnal JV, Rueckert D. Fast fully automatic brain detection in fetal MRI using dense rotation invariant image descriptors. 2014 IEEE 11th International Symposium on Biomedical Imaging (ISBI); 2014. p. 1230–3.

[21] Styner M, Oguz I, Xu S, Brechbuhler C, Pantazis D, Levitt JJ, Shenton ME, Gerig G. Framework for the statistical shape analysis of brain structures using SPHARM-PDM. Insight J 2006;1071:242–50.
[22] Chung MK, Dalton KM, Davidson RJ. Encoding neuroanatomical information using weighted spherical harmonic representation. 2007 IEEE/SP 14th Workshop on Statistical Signal Processing2007; p. 146-150.
[23] Zhou H, Li L. Regularized matrix regression. J R Stat Soc Series B 2014;76:463–83.
[24] Holm S. A simple sequentially rejective multiple test procedure. Scand J Stat 1979;6:65–70.
[25] Beddy P, O'Neill AC, Yamamoto AK, Addley HC, Reinhold C, Sala E. FIGO staging system for endometrial cancer: added benefits of MR imaging. Radiographics 2012;32:241–54.
[26] Nakaura T, Higaki T, Awai K, Ikeda O, Yamashita Y. A primer for understanding radiology articles about machine learning and deep learning. Diagn Interv Imaging 2020;101:765–70.
[27] Chen X, Wang Y, Shen M, Yang B, Zhou Q, Yi Y, et al. Deep learning for the determination of myometrial invasion depth and automatic lesion identification in endometrial cancer MR imaging: a preliminary study in a single institution. Eur Radiol 2020;30:4985–94.
[28] Dong HC, Dong HK, Yu MH, Lin YH, Chang CC. Using deep learning with convolutional neural network approach to identify the invasion depth of endometrial cancer in myometrium using MR images: a pilot study. Int J Environ Res Public Health 2020;17:5993.
[29] Urushibara A, Saida T, Mori K, Ishiguro T, Inoue K, Masumoto T, et al. The efficacy of deep learning models in the diagnosis of endometrial cancer using MRI: a comparison with radiologists. BMC Med Imaging 2022;22:80.
[30] Parmar C, Grossmann P, Bussink J, Lambin P, Aerts HJWL. Machine learning methods for quantitative radiomic biomarkers. Sci Rep 2015;5:13087.
[31] Ytre-Hauge S, Husby JA, Magnussen IJ, Werner HM, Salvesen OO, Bjorge L, et al. Preoperative tumor size at MRI predicts deep myometrial invasion, lymph node metastases, and patient outcome in endometrial carcinomas. Int J Gynecol Cancer 2015;25:459–66.
[32] Nakamura K, Nakayama K, Ishikawa N, Minamoto T, Ishibashi T, Ohnishi K, et al. Preoperative tumor size is associated with deep myometrial invasion and lymph node metastases and is a negative prognostic indicator for patients with endometrial carcinoma. Oncotarget 2018;9:23164–72.